remote sensing

MDPI

Article

Estimating Snow Water Equivalent with Backscattering at X and Ku Band Based on Absorption Loss

Yurong Cui [1], Chuan Xiong [1,*], Juha Lemmetyinen [2], Jiancheng Shi [1], Lingmei Jiang [3], Bin Peng [1], Huixuan Li [4], Tianjie Zhao [1], Dabin Ji [1] and Tongxi Hu [1]

1 State Key Laboratory of Remote Sensing Science, Institute of Remote Sensing and Digital Earth, Chinese Academy of Sciences, Beijing 100101, China; cuiyr@radi.ac.cn (Y.C.); shijc@radi.ac.cn (J.S.); pengbin@radi.ac.cn (B.P.); zhaotj@radi.ac.cn (T.Z.); jidb@radi.ac.cn (D.J.); hutx@radi.ac.cn (T.H.)
2 Finnish Meteorological Institute, P.O. Box 503, Helsinki Fin-00101, Finland; juha.lemmetyinen@fmi.fi
3 State Key Laboratory of Remote Sensing Science, Beijing Normal University, Beijing 100875, China; jiang@bnu.edu.cn
4 Department of Geography, University of South Carolina, Callcott Building 709 Bull Street, Columbia, SC 29208, USA; lihuixuan90528@gmail.com
* Correspondence: xiongchuan@radi.ac.cn; Tel.: +86-10-6480-7983

Academic Editors: Wolfgang Wagner and Prasad S. Thenkabail
Received: 9 March 2016; Accepted: 3 June 2016; Published: 16 June 2016

Abstract: Snow water equivalent (SWE) is a key parameter in the Earth's energy budget and water cycle. It has been demonstrated that SWE can be retrieved using active microwave remote sensing from space. This necessitates the development of forward models that are capable of simulating the interactions of microwaves and the snow medium. Several proposed models have described snow as a collection of sphere- or ellipsoid-shaped ice particles embedded in air, while the microstructure of snow is, in reality, more complex. Natural snow usually forms a sintered structure following mechanical and thermal metamorphism processes. In this research, the bi-continuous vector radiative transfer (bi-continuous-VRT) model, which firstly constructs snow microstructure more similar to real snow and then simulates the snow backscattering signal, is used as the forward model for SWE estimation. Based on this forward model, a parameterization scheme of snow volume backscattering is proposed. A relationship between snow optical thickness and single scattering albedo at X and Ku bands is established by analyzing the database generated from the bi-continuous-VRT model. A cost function with constraints is used to solve effective albedo and optical thickness, while the absorption part of optical thickness is obtained from these two parameters. SWE is estimated after a correction for physical temperature. The estimated SWE is correlated with the measured SWE with an acceptable accuracy. Validation against two-year measurements, using the SnowScat instrument from the Nordic Snow Radar Experiment (NoSREx), shows that the estimated SWE using the presented algorithm has a root mean square error (RMSE) of 16.59 mm for the winter of 2009–2010 and 19.70 mm for the winter of 2010–2011.

Keywords: snow water equivalent; active microwave remote sensing; bi-continuous; X and Ku

1. Introduction

Snow cover can reflect a large part of incident solar radiation because of its high albedo and a large amount of water resources store in the snowpack, which are the primary source of water for river channel discharge in the middle-to-high latitude areas. Therefore, snow cover has a great impact on the surface energy budget of the Earth, as well as global and regional water cycles [1–3]. Moreover, one sixth of the total population of the word depends on snowmelt runoff to meet their

fresh water needs [4] and for agricultural irrigation requirements. In some drainage basins, rapid spring snowmelt may also cause flooding and thus predicting the runoff resulting from snowmelt is an important part of the flood control system [5]. As a result, there is an urgent demand for quantitative methods to estimate snow water equivalent (SWE) and snow depth, providing information for disaster mitigation, snow water resources management and climate monitoring.

Due to the inhomogeneous distribution of snow cover on the surface of the Earth, traditional *in situ* measurement techniques can hardly provide sufficient coverage of snow information. In the last few decades, remote sensing has proven to be an important technique for observing snow cover at large scales. Optical and near-infrared remote sensing have been successfully applied to snow cover mapping at relatively high spatial resolutions [6]. However, these observations are often affected by poor weather and insufficient lighting conditions. Microwave remote sensing can obtain snowpack information for all time and weather conditions because of its target-penetrating abilities [7]. Especially, active radars with high spatial resolution are very promising to estimate snow parameters such as snow depth, snow density and grain size [8,9]. Many previous studies have made a first attempt at snowpack measurements by active microwave remote sensing (AMRS). Based on snow pile experiments, Ulaby and Stiles [8,10] demonstrated the potential use of AMRS for measuring SWE. Moreover, they directly established a positive relationship between SWE and backscattering signals at 8.6 and 35 GHz with a simple backscattering model. Shi estimated snow density [11] and snow depth as well as particle size [9] using SAR at the relatively low frequencies of L, C and X band, which exhibit a large penetration depth. Theoretical studies and experiments have also been carried out to explore the relationship between snow volume backscattering and snow physical parameters. It has been demonstrated that high frequency radar is more applicable for snow monitoring as higher frequency bands were found to be more sensitive to snow parameters [12,13]; in particular, the snow backscattering signal at Ku band is more sensitive than that at X and C bands [14]. Shi [15] found that more snow volume signals are generated at Ku band than at lower frequencies, and it is more sensitive to snow cover by simulating the relationship between optical thickness and albedo with a theoretical model. Shi [16] explored the ideas of snow water equivalent retrieval with the combination of the X (9.6 GHz) and Ku (17.2 GHz) bands. Pettinato [17] presented a case study of SWE retrieval from X band. The Cold Regions Hydrology high-resolution Observatory (CoReH2O) [18], a candidate for the 7th Earth Explorer missions, selected by the ESA for Phase-A studies in 2009, aimed at filling gaps in current knowledge for snow monitoring with the configuration of X and Ku bands. However, the mission was finally not selected for implementation. The Water Cycle Observation Mission (WCOM) in China [19] has been proposed to simultaneously monitor soil moisture, SWE, soil freeze-thaw process and some other variables on an integrated platform. Combined active and passive microwave sensors with wide frequency coverage are onboard WCOM. There will be three main payloads onboard the WCOM: (1) An L-S-C tri-frequency full-polarized Interferometric Microwave Imager (IMI) with spatial resolution ranging from 15 km to 50 km for soil moisture and ocean salinity; (2) A Polarized Microwave Imager (PMI) covering 6.8 to 150 GHz band with a 1.8 m diameter reflector antenna for conical scan. Most of its frequency channels have the capability of full-polarizations; (3) An X-Ku Dual-Frequency Polarized Microwave Scatterometer (DPS) with 2~5 km resolution and 1000 km swath for snow water equivalence and freeze-thaw mapping. For SWE estimation, an X and Ku band dual-frequency polarized scatterometer is planned, in a similar configuration as CoReH2O but with 2~5 km spatial resolution and improved global coverage. Simulation of the ground backscattering signals from snow covered surfaces with the configurations of CoReH2O and WCOM missions is critical for concept demonstration. Monitoring the phase of the radar signal also gives the possibility to track SWE by means of repeat-pass interferometry [20,21]. While providing accurate retrievals on a local scale, global applications would require an improvement of available repeat-pass SAR coverage compared to existing systems (e.g., TerraSAR-X, TanDEM-X).

Theoretical models can improve our understanding of the interaction mechanism between electromagnetic waves and the snowpack, and thus can guide us to estimate snow parameters from

measurements of backscattering intensity. Initial theoretical models based on the traditional vector radiative transfer equation described the snow particles as spheres or ellipsoids and assumed that the scattering from snow particles was independent, and the intensity of total scattering was the sum of that from each particles ignoring the collective scattering effect of particles. However, as snow depth and density increase, multiple scattering effects become more significant. In order to consider the interactions among snow particles, Tsang *et al.* [22] proposed the Dense Media Radiative Transfer (DMRT) approach based on quasi-crystalline approximation (QCA), considering the snow pack as dense medium consisting of partially merged particles. Further, Du *et al.* [23] developed a multi-scattering and multi-layer snow scattering model with Matrix Doubling method. The verification of this model showed consistency with measured data [24]. However, their study still underestimated the backscattering signals at cross polarization since the shapes of snow particles were still considered as spheres or ellipsoids. In this study, the bi-continuous vector radiative transfer (bi-continuous-VRT) model, which can construct snow microstructure to resemble true shapes found in natural snowpacks [25], is used to simulate the scattering characteristics from the snowpack. The model is applied to simulate snow volume scattering, while Advanced Integral Equation Model (AIEM) [26] is applied to simulate the soil surface backscattering under snow cover. We utilize this integrated theoretical model for backscattering simulation of snow covered ground to construct a backscattering database, and to develop our new parameterization scheme for volume scattering, applied in a SWE retrieval algorithm.

The main objective of this study is to demonstrate the estimation of SWE from X and Ku band active microwave observations, by using the bi-continuous-VRT model. Following this introduction, Section 2 describes the theoretical forward model (bi-continuous-VRT model) for backscattering simulation from snow-covered ground and the model validation with SARALPS 2007 data [27]. In Section 3, the method of SWE retrieval is described. The dataset used for the SWE retrieval algorithm validation is described in Section 4 and the retrieved results and analysis are discussed in Section 5. The final section summarizes our work.

2. Snowpack Backscattering Simulation

2.1. The Theoretical Forward Model for Backscattering from Snowpack

Radar backscattering signals over snow-covered ground at a given incidence angle θ_i can be considered to consist of four components: the surface scattering component from the air–snow interface $\sigma^a_{pq}(f)$, a volume scattering component from snowpack $\sigma^{vol}_{pq}(f)$, the interaction component between snow volume and snow-ground interface $\sigma^{vg}_{pq}(f)$, and the direct ground scattering component $\sigma^g_{pq}(f)$, so that

$$\sigma^{tol}_{pq}(f) = \sigma^a_{pq}(f) + \sigma^{vol}_{pq}(f) + \sigma^{vg}_{pq}(f) + T^2_{pq} \cdot L^2_{pq} \cdot \sigma^g_{pq}(f) \quad (1)$$

where

$$L_{pq} = \exp(-\tau/\mu) \quad (2)$$

$$\mu = \cos\theta_r \quad (3)$$

$$\tau = ke \cdot d \quad (4)$$

and f is the radar frequency, at polarization $p\,q$, T_{pq} is the power transmission coefficient at the air–snow interface (close to unity for dry snow), θ_r is the refraction angle caused by the presence of snow, and L_{pq} is the snow volume attenuation factor. The optical thickness τ is the product of the snow extinction coefficient k_e and snow depth d. We utilize the bi-continuous-VRT model to simulate the backscattering from snowpack and the AIEM model to simulate the direct ground backscattering component at co-polarizations (VV and HH polarizations) and Oh model [28] for that at VH polarization.

The bi-continuous-VRT model firstly simulates bi-continuous random structures by the level-cut method, which is more similar to real snow structure. Then, the scattering parameters (scattering

coefficient, absorption coefficient, scattering phase matrix, *etc.*) calculated from the simulated incoherent scattered field are coupled to the radiative transfer equation. The polarimetric backscattering coefficient can then be obtained after solving the radiative transfer model.

For the soil backscattering model, one of the most popular models for soil surface backscattering at co-polarizations is the AIEM, which is more complex than other traditional surface scattering models, such as the Small Perturbation Model, Geometry Optical Model and Physical Optical Model. AIEM is an improved version of the Integral Equation Model (IEM) [29], which has been verified against experimental *in-situ* data [23,30]. For simulating the cross-polarization backscattering of bare soil, an empirical Oh model was developed based on polarimetric radar measurements with measured soil surface root mean square height (RMS height), correlation length, and dielectric constant [28]. Several soil surface parameters (soil surface RMS height, surface correlation length, soil moisture content and auto-correlation function) are needed to do the surface backscattering simulation.

Signals from the air–snow surface can be ignored because for dry snow, these are very small compared with other scattering components at off-nadir incidence [31]. The snow volume backscattering simulated by the bi-continuous-VRT model also includes the interaction component between snow volume and snow-ground interface. When the power transmission coefficient at the air–snow interface is assumed to be unity, Equation (1) can be expressed as:

$$\sigma_{pq}^{tol}(f) = \sigma_{pq}^{g}(f)\exp(-2\tau/\mu) + \sigma_{pq}^{vol}(f) \quad (5)$$

Input parameters of the forward model described in Equation (5) include optical grain size, grain size distribution parameter, snow depth, snow density for the snow volume backscatter simulation and soil surface RMS height, soil correlation length, and soil moisture content for the ground surface backscatter simulation. Specifically, the optical grain size R_e, grain size distribution parameter "b" and snow density are the input parameters to characterize the snow microstructure in bi-continuous-VRT model [25]. The optical grain size R_e is defined as the grain size of identical spheres which have the same specific surface area (SSA) as the bicontinuous medium, which can be analytically derived. The grain size distribution parameter b is an indicator of grain size distribution. As b decreases, the clustering effect becomes stronger and aggregation effects are stronger [32].

In previous theoretical models, most surfaces have been considered to have only one scale of roughness. However, the natural land surface is very complex and usually contains multiple roughness scales. To recognize a scale, the coherence of the backscattered signal over the scale must be retained. For a multiscale rough surface, only a range of roughness scales is effective in generating scattering at a given view angle and a frequency [33]. Because of this, microwave at centimeter wavelength, may sense only roughness scales smaller or comparable to the wavelength at mid- or large-incident angles [29]. Thus, considering a frequency range from X to Ku band, we take into account soil surface RMS height values from 0.001 cm to 0.1 cm in the process of backscattering simulation.

Taking all of the above factors into consideration, we generated a simulated database through running the bi-continuous-VRT model: a wide range of snow parameters (snow depth, particle size, volume fraction of ice, particle, and size variation, *etc.*) and soil roughness conditions (soil surface RMS height, soil correlation length) are considered; a nominal incident angle of 40° at X and Ku bands is used, considering also the impact of snow density [34] on incident angle at the snow surface. The ranges and intervals for the model parameters are shown in Table 1. Considering most of the ground surface under dry snow cover is in the frozen state, soil moisture of ground is assumed to be 0.02 (m^3/m^3), which can be considered as realistic based on *in situ* measurements [32].

Table 1. Snow and underground parameters used to generate the database.

Parameters	Minimum	Maximum	Interval
Optical grain radius (mm)	0.1	0.6	0.1
b parameter	0.5, 1.2, 2.5, 4.5, 6.5, 8.5, 10, 50, 90		
Ice fraction	0.15	0.45	0.1
Snow depth (m)	0.1	1.7	0.4
Soil RMS height (cm)	0.001	0.1	0.001
Soil correlation length (cm)	1.0	23	2.0

2.2. Model Validation with SARALPS-2007 Data

In this section, the theoretical forward backscattering model for snow covered ground described in Equation (5) is demonstrated against the SARALPS-2007 field experimental data from ESA (European Space Agency). Aimed at validation of the backscatter models and the development of snow retrieval algorithms, this experimental campaign collected fully polarimetric backscattering data of snow-covered ground at X and Ku bands (10 GHz and 17 GHz) with a ground-based Synthetic Aperture Radar (GB-SAR), operated with a variety of incident angles (from 30° to 70°). Kűhtai site located in a side valley above the Inn valley about 30 km southwest of Innsbruck is selected for the backscattering model simulation. Meteorological datasets are available from adjacent meteorological stations. A relatively flat meadow was used as the test site. Snow measurements were made at several locations within or close to the GB-SAR footprint. The prevailing snow conditions and GB-SAR data are described for each of the seven campaign days [27]. However, there are only two observations for dry snow on 17 January and 5 February at Kűhtai/Untere Issalm test site. There was no HH polarization measurement available for 17 January. The detailed descriptions of the field measurements are summarized in Table 2. Because the backscattering at cross polarization from underground at X and Ku band is underestimated by the Oh model [28], a scale factor is introduced in the Oh model for cross-polarization backscattering simulation in order to match the cross-polarization backscattering observations of the bare soil under snow cover. We simulate the backscattering at different incident angles (30°, 40°, 50°, 60°) using the integrated theoretical model and compare the simulated results with GB-SAR observations. Soil surface roughness parameters were obtained from laser profiler and a roughness plate measurements; the snow density and snow depth values were obtained from snow pit observations. The performance of the model is assessed by comparison to measured signatures in dry snow conditions.

Table 2. SARALPS-2007 field measurements of snow properties on 17 January and 5 February.

Parameters	17 January	5 February
RMS height of ground surface	0.95 cm	0.95 cm
Correlation length of ground surface	18 cm	18 cm
Soil moisture of ground	0.05 m^3/m^3	0.05 m^3/m^3
Snow depth	38 cm	36.6 cm
Snow density	260.5 kg/m^3	278.0 kg/m^3

Figure 1 shows the comparison of the GB-SAR data with the model predictions on 17 January and 5 February 2007. For the snow volume backscattering simulation, the optical grain size R_e was 0.2 mm, the *b* parameter was set to be 1.2. For the ground backscattering simulation, the soil RMS height was 0.95 cm, correlation length was 3.8 cm and the volumetric moisture mv was 0.02 m^3/m^3. This result shows reasonably good agreement for co-polarized backscatter at X and Ku bands between the forward model simulations and observations. Table 3 shows the comparison between simulated backscattering and observed backscattering. R^2 stands for coefficient of determination. RMSE means root mean square error. The model accurately simulates the observed decreasing trend of backscattering with increased incident angles at both two bands. Figure 1 also shows that the backscattering at Ku band is higher than that at X band.

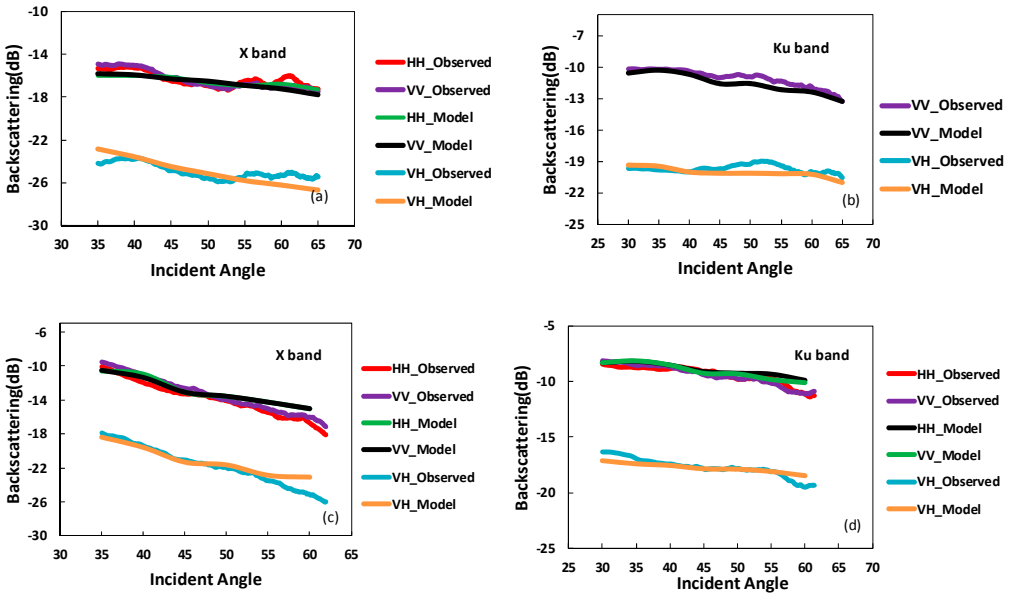

Figure 1. Comparison of the GB-SAR observed with the model predicted backscattering on 17 January 2007 (**a**) at X band and (**b**) at Ku band; and 5 February 2007 (**c**) at X band and (**d**) at Ku band.

Table 3. Comparison between simulated backscattering and observed backscattering.

		X Band			Ku Band		
		VV	**HH**	**VH**	**VV**	**HH**	**VH**
17 January	R^2	0.83	0.80	0.82	0.93	-	0.80
	RMSE	0.52 dB	0.48 dB	0.83 dB	0.48 dB	-	0.55 dB
	p-value	0.0044	0.0242	0.0130	0.0001	-	0.0340
5 February	R^2	0.95	0.94	0.94	0.92	0.96	0.96
	RMSE	0.7 dB	0.98 dB	0.85 dB	0.48 dB	0.59 dB	0.50 dB
	p-value	0.0001	0.0012	0.0008	0.0005	0.0027	0.0001

2.3. Impacts of Grain Size on the Simulated Snowpack Backscattering

Optical grain size of bi-continuous medium here means equal surface-to-volume ratio compared with spheres [35]. In this part, the simulated scattering properties of the snowpack at X and Ku bands are analyzed, using the created database of simulations (Table 1). The total scattering at Ku band is dominated by the snow volume scattering, so the effects of snow volume scattering are more significant at Ku band than that at X band up to 7 dB [36]. Moreover, the larger optical thickness at Ku band leads to a smaller one-way penetration depth (~3–4 m) than that at X band (in the order of 10 m). Figure 2 shows VV-polarized signals at Ku and X bands simulated by the bi-continuous-VRT model, varying with snow depth and optical grain size R_e (corresponding to the radius of snow grains), snow density and small soil moisture. Figure 2 shows the signals of X and Ku bands at VV polarization both increasing with snow depth. As expected, the simulated signal at Ku band is stronger than that at X band because of the higher sensitivity to snow scattering properties at a higher frequency. This is also consistent with the findings from Figure 1. The result also shows that optical grain size R_e has a significant effect on snow backscattering under constant *b* parameter of 1.2 as the difference between the simulated signals for the lowest (0.1 mm) and biggest (0.6 mm) R_e is more than 15 dB at both two bands, while the dynamic range for an increase of 1.5 m is in the order of 10 dB.

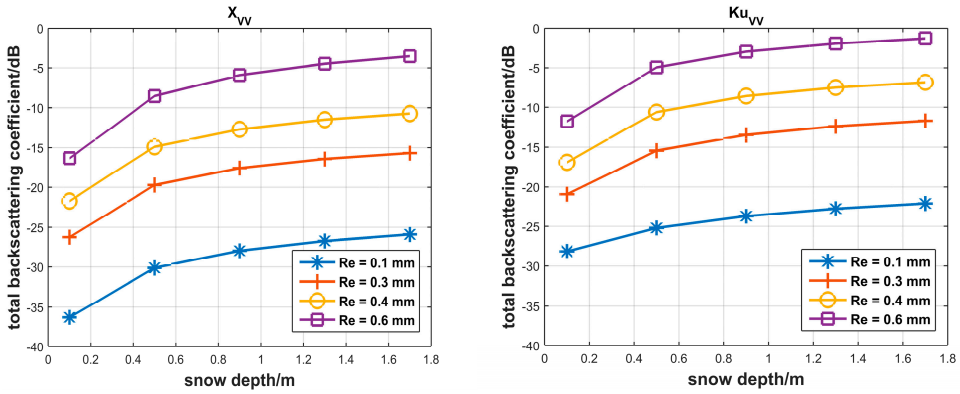

Figure 2. Total backscattering coefficient from dry snow at X (**left**) and Ku (**right**) bands with VV polarization and incidence angle of 40° against increase in snow depth. The values of 0.1 mm, 0.3 mm, 0.4 mm and 0.6 mm were applied for the optical grain size R_e. The b parameter was 1.2.

3. Retrieval Method

3.1. Snow Volume Scattering Model Simplification

Theoretical models need numerous input quantities and high computational efficiency; thus these typically cannot be directly used in the inverse problem. Parameterization aims to minimize the number of unknown variables and improve the retrieval efficiency, while retaining a known accuracy. To enable retrieval, we parameterized snow volume signals generated from the bi-continuous-VRT model in which multiple scattering mechanisms have been taken into consideration, using the database of simulations described in Table 1.

As shown in Figure 3, the cosine of incident angle μ under different snow density has little impact on the relationship between optical thickness and the attenuation factor. Therefore, μ caused by the presence of snow is set to a constant value of 0.8467, which is the mean value when the most of snow densities ranging from 0.05 to 0.45 g/cm^3, to simplify the bi-continuous-VRT model for inversion.

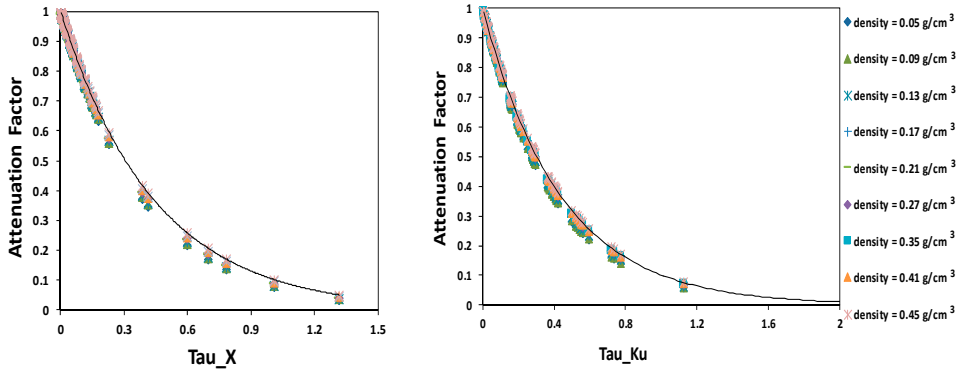

Figure 3. The attenuation factor for different snow densities for X (**left**) and Ku (**right**) bands.

Although the first order solution of the radiative transfer equation does not consider multiple scattering effects, it forms the major part of snow volume backscattering signals [37]. Therefore, we utilize the first-order solution to parameterize the snow volume scattering. The first-order solution of snow volume backscattering is shown in Equation (6) [38]. The parameterized formulas for snow volume scattering at X and Ku bands are shown in Equations (7)–(10), respectively. The coefficients in Equations (7)–(10) are obtained through least square regression and the parameter values are shown in Table 4.

$$\sigma_0^{vol} = 0.75\mu\omega\left(1 - \exp\left(-2\tau/\mu\right)\right) \quad (6)$$

$$\sigma_{X_{vv}}^{vol} = p_1^{X_{vv}} \sigma_0^{vol} (X_{vv})^2 + p_2^{X_{vv}} \sigma_0^{vol} (X_{vv}) + p_3^{X_{vv}} \quad (7)$$

$$\sigma_{Ku_{vv}}^{vol} = p_1^{Ku_{vv}} \sigma_0^{vol} (Ku_{vv})^2 + p_2^{Ku_{vv}} \sigma_0^{vol} (Ku_{vv}) + p_3^{Ku_{vv}} \quad (8)$$

$$\sigma_{X_{vh}}^{vol} = p_1^{X_{vh}} \sigma_0^{vol} (X_{vh})^2 + p_2^{X_{vh}} \sigma_0^{vol} (X_{vh}) + p_3^{X_{vh}} \quad (9)$$

$$\sigma_{Ku_{vh}}^{vol} = p_1^{Ku_{vh}} \sigma_0^{vol} (Ku_{vh})^2 + p_2^{Ku_{vh}} \sigma_0^{vol} (Ku_{vh}) + p_3^{Ku_{vh}} \quad (10)$$

Table 4. Coefficients for Snow Volume Scattering Parameterization.

Coefficients (X)	Value	Coefficients (Ku)	Value
$p_1^{X_{vv}}$	−0.0009	$p_1^{Ku_{vv}}$	0.0038
$p_2^{X_{vv}}$	1.0093	$p_2^{Ku_{vv}}$	1.1871
$p_3^{X_{vv}}$	−1.0191	$p_3^{Ku_{vv}}$	0.4267
$p_1^{X_{vh}}$	0.006	$p_1^{Ku_{vh}}$	0.0118
$p_2^{X_{vh}}$	1.3933	$p_2^{Ku_{vh}}$	1.6587
$p_3^{X_{vh}}$	−10.176	$p_3^{Ku_{vh}}$	−8.0115

Single scattering albedo ω is the ratio of scattering coefficient k_s and the sum of absorption coefficient k_a and the scattering coefficient k_s in Equation (6). Figure 4 demonstrates a comparison of the result of parameterized volume backscattering component based on Equations (7)–(10) to that of simulated one from the bi-continuous-VRT model with R^2 of 0.94, RMSE of 1.57 dB and Bias of 1.18 dB at X band VV polarization; R^2 of 0.90, RMSE of 0.96 dB and Bias of 0.72 dB at X band VH polarization; R^2 of 0.96, RMSE of 1.35 dB and Bias of 1.07 dB at Ku band VV polarization; and R^2 of 0.96, RMSE of 1.03 dB and Bias of 0.81 dB at Ku band VH polarization. The parameterization scheme has very good performance at both frequency bands, while performing slightly better at Ku band than at X band because the interaction component between snow volume and snow-ground interface at the longer wavelength X band is stronger than that at the shorter wavelength Ku band, which cannot be expressed well by the first-order solution of snow volume backscattering shown in Equation (6).

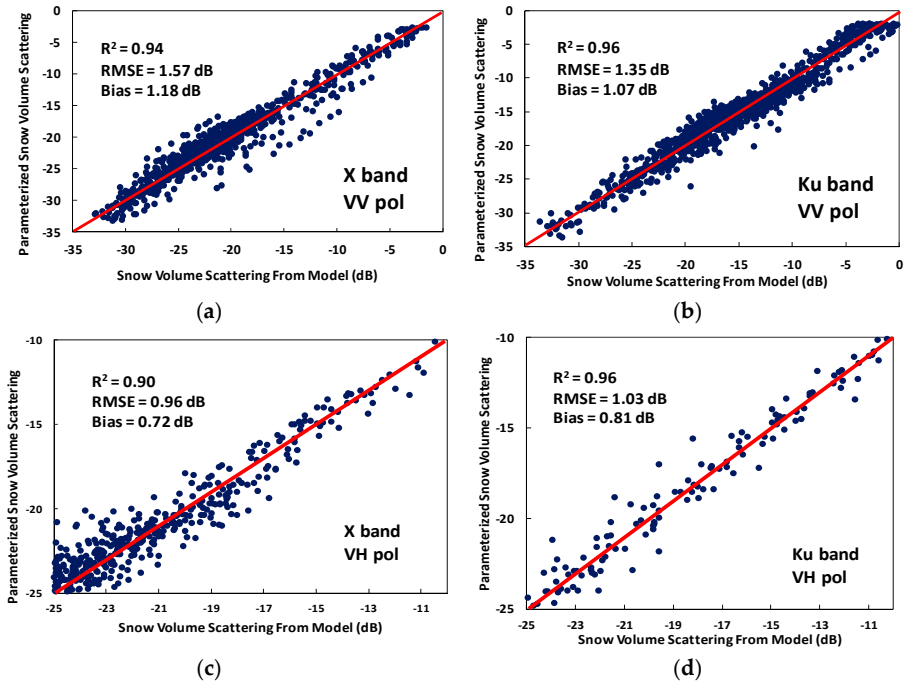

Figure 4. Comparing the simulated snow volume backscattering of X at VV (**a**) and VH (**b**) polarizations; and that of Ku at VV (**c**) and VH (**d**) polarizations with the ones calculated by Equations (7)–(10), respectively.

3.2. Relationships of Albedo and Optical Thickness at X and Ku Bands

Figure 5 demonstrates the relationships of single scattering albedo and snow optical thickness at X and Ku bands. The snow scattering characteristics at X and Ku bands, as simulated by the bi-continuous-VRT model, are highly correlated. It is thus possible to find the relationships of snow property parameters between these two bands. Based on the database generated by the model, the following relationships of optical thickness and single scattering albedo between Ku and X bands were founded:

$$\tau_{Ku} = 5.3178\tau_X - 0.0225 \tag{11}$$

$$\omega_{Ku} = -0.9060{\omega_X}^2 + 1.9366\omega_X - 0.0808 \tag{12}$$

The fitted relationships, shown in Figure 5, have R^2 of 0.9627 for single scattering albedo and R^2 of 0.9962 for optical thickness.

Based on these parameterization forms of snow volume backscattering in Equations (7)–(10), and the relationships of scattering parameters between single scattering albedo and the optical thickness at X and Ku bands Equations (11) and (12), respectively—snow volume backscattering at Ku band can be expressed by snow volume backscattering at X band. Thereby the number of unknown variables would be reduced in the process of SWE estimation.

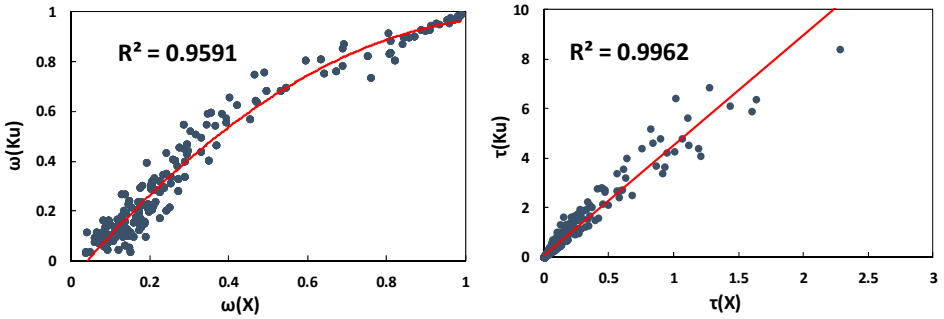

Figure 5. The relationship between single scattering albedo at X band and that at Ku band (**left**) and the relationship between the snow optical thickness at X bands and at Ku band (**right**).

3.3. Cost Function

The estimation of geophysical parameters from satellite data is hampered by uncertainties of the complicated geo system and mutual influences of parameters in this system. It is very popular to use statistical methods to retrieve geophysical variables [39,40], such as the least square method (LSM). In this approach, the target parameter is retrieved through iteratively minimizing a cost function that describes the difference between the simulated and observed signals. We test two different cost functions: one does not have any prior knowledge about the parameters as shown in Equation (13):

$$F = \sum_{i=1}^{4} \frac{\left[\sigma_i^{meas} - \sigma_i^{\mathrm{model}}(x_1, x_2)\right]^2}{2\mathrm{var}_i^2} \tag{13}$$

The other one is built with *a priori* constraint, as shown in Equation (14), that was also used in the proposed CoReH2O SWE retrieval algorithm, where an a priori constraint was applied for the effective grain radius [41]:

$$F = \sum_{i=1}^{4} \frac{\left[\sigma_i^{meas} - \sigma_i^{\mathrm{model}}(x_1, x_2)\right]^2}{2\mathrm{var}_i^2} + \sum_{i=1}^{2} \frac{[x_i - \overline{x_i}]^2}{2\lambda_i^2} \tag{14}$$

where i represents the number of the measurement channel (X and Ku bands at VV, VH polarizations), x_i denotes albedo and optical thickness, respectively, σ_i^{meas} denotes the measured backscattering signals, and $\sigma_i^{\mathrm{model}}$ denotes the modeled backscattering signals which is the function of albedo and

optical thickness. var_i^2 is the expected error variance of the measurements which can be obtained from the sensor configuration. Here, 0.5 dB was used from the document of CoReH2O. $\overline{x_i}$ in Equation (14) represents the reference value for albedo and optical thickness which is usually roughly estimated from backscattering coefficient, or estimated from other sources (such as a snow process model). λ_i^2 is the variance of x_i which affects the weight of constraints in the cost function. According to statistical theory, the value of x_i then mostly ranges from $\overline{x_i} - 2\lambda_i$ to $\overline{x_i} + 2\lambda_i$ with x_i assumed to obey normal distribution [39].

We firstly compare these two cost functions in Equations (13) and (14) in their abilities of global convergence for the unknowns. Figure 6 shows two-dimensional contour plots of these cost function Equations (13) and (14) when varying the albedo and optical thickness values. The reference value in Figure 6a is based on simulations generated from the bi-continuous-VRT model. We can see that, with the increase of the number of iterations, the cost function with constraints gradually converges to the solution of the two parameters. However, when cost function with no constraint is used, the contour lines spread across the whole range of variable interval with increasing iteration number, as shown in Figure 6b. Therefore, the cost function with constraints will be utilized in later SWE estimation. With the Equations (7)–(12), the snow scattering parameters τ_x and ω_x can be obtained by minimizing the cost function.

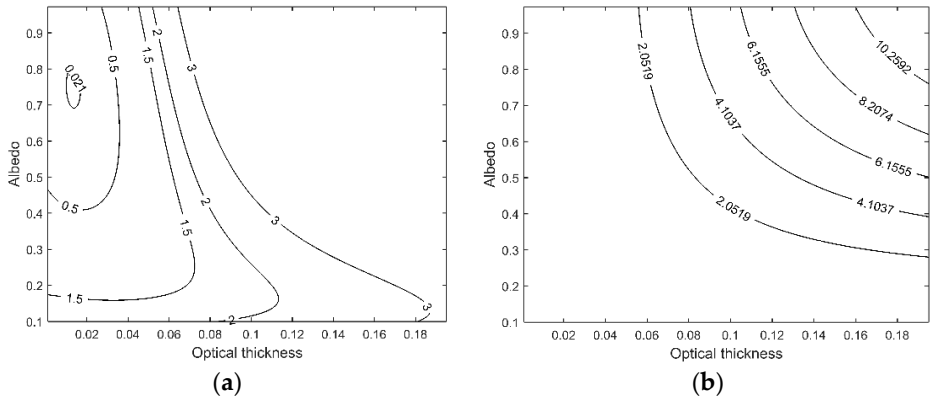

Figure 6. The contours of cost function with constraints (**a**) and without constraints (**b**), using a simulated test case.

3.4. Estimation of SWE

The snow optical thickness is a product of snow depth and the extinction coefficient, which is closely related to SWE. The absorption part of snow optical thickness τ_a is a product of the snow absorption coefficient and snow depth, which is linearly related to SWE [16]. τ_a can be calculated by the optical thickness and albedo retrieved in the last part shown as Equation (14):

$$\tau_a\left(fre\right) = \left(1 - \omega_{fre}\right) \cdot \tau_{fre} = k_a\left(fre\right) d \tag{15}$$

The absorption coefficient k_a can be empirically described as [42]:

$$k_a = V_s k_0 \frac{\xi''}{\xi} \left| \frac{3\xi}{\xi_i + 2\xi} \right|^2 \tag{16}$$

where, k_0 is the radar wave number, ξ is the dielectric constant of the background (ξ = 1 for air and ξ_i = 3.15 for ice), ξ'' is the imaginary part of the dielectric constant of ice that is mainly determined by snow temperature, and Vs is volume fraction of ice (snow density $\rho_s = 0.917Vs$). Figure 7 shows that the empirically estimated k_a through Equation (16) matches very well with the ones simulated by the theoretical the bi-continuous-VRT model. Therefore, Equation (16) can be used in SWE estimation.

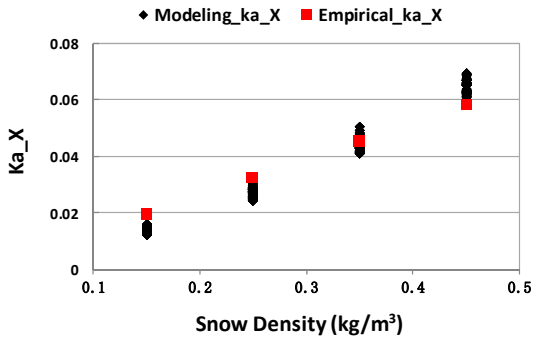

Figure 7. Comparison between the empirically estimated absorption coefficient through Equation (16) and the one simulated by the bi-continuous-VRT model.

According to Equations (15) and (16), SWE can be expressed in the following form Equation (17):

$$SWE = \tau_a\,(fre) \cdot \frac{0.917}{0.339 k_0 \xi''_{ice}\,(fre)} \tag{17}$$

The imaginary part of dielectric constant of ice can be described as [43]:

$$\xi''_{ice}\,(fre) = \frac{0.96\left(\frac{fre}{8.5}\right)}{1226 - 32.8 T_{ice}} \tag{18}$$

where T_{ice} is the ice temperature in Centigrade. As is apparent from Equations (17) and (18); snow temperature has a direct influence on the snow absorption coefficient. In order to characterize the influence of snow temperature on the SWE estimation, different snow temperatures were used to calculate SWE under the fixed value of τ_a using Equations (17) and (18). The result is shown in Figure 8. The results show that with a temperature change of two degrees, the SWE changes about 5 mm. In this study, we postulate that snow temperature can be assumed to be a constant value in the SWE inversion, considering the typically low variability of snow physical temperature (with the exception of shallow snow and snow surface layers for deeper snow), arising from the high insulating properties of snow. Moreover, the snow temperature can be determined from snow physical models and reanalysis data; in this case, the snow temperature can be more accurate.

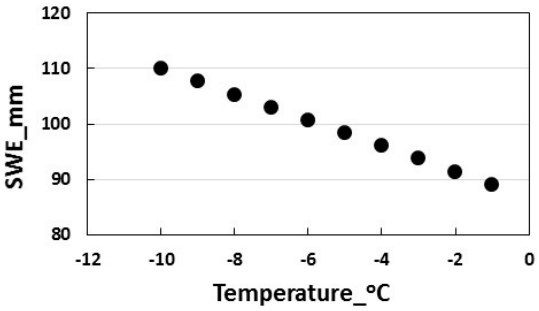

Figure 8. The relationship between temperature and SWE at X band under the fixed absorption part of optical thickness 0.0057 at X band.

Before SWE is calculated, the surface backscattering signals need to be removed from the total backscattering. We assume that the roughness of the soil surface is constant and ground surface below is in a frozen state during the whole winter. The backscatter before snowfall or during the early snow covered period when the snowpack is thin is dominated by the signal from the snow/ground interface. We regard this as the ground backscattering signal.

4. NoSREx Experimental Dataset

In the NoSREx experiment, a time series active and passive microwave measurements of snow cover were carried out with a ground-based scatterometer and several radiometers [44]. The measurements were conducted at the Arctic Research Centre of the Finnish Meteorological Institute (26°38.270′E; 67°21.712′N) near the town of Sodankylä in Northern Finland between October 2009 and May 2013. The test area was located in a forest clearing. The soil at the site consists of mineral soil covered by a thin layer of organic matter (~5 cm) as surface vegetation consisting of small shrubs, grass and lichen. Brightness temperature at 1.4, 10.65, 18.7 and 37 GHz, H and V pol, at four incident angles (30°, 40°, 50°, and 60°) was measured by the SodRad system. Average value and standard deviation of each elevation scan were provided. The X and Ku bands polarimetric backscattering coefficient was measured by the SnowScat system, a ground-based, fully polarimetric frequency step radar [45]. The main characteristics of SnowScat are given in Table 5. SnowScat was mounted at a height of 9.6 m overlooking the clearing, allowing scans of the measurement area both in elevation and azimuth. Four elevations, providing 30, 40, 50 and 60 degree incidence angles from nadir at ground level, were measured. The nominal scan consisted of 17 discrete azimuth directions at each elevation. In this study, VV polarized backscattering signals at 10.6 GHz and 16.7 GHz with 40° incident angle were used for estimation of SWE. All scans in the azimuth were averaged to provide a single value of backscattering corresponding to a given scan in elevation. We focus on data from the first two seasons of the experiment. SnowScat scans took place every three hours during the first season. The measurement period was extended to four hours from the second season onwards.

Table 5. SnowScat Characteristics.

Parameter	Nominal Observations
Frequency range	9.2–17.8 GHz
Polarizations	HH, HV, VH, VV
Elevation scan range	30°~60° *
Elevation scan step	10°
Number of elevation steps	4
Azimuth range **	−166°~−142°
Azimuth step	6°
Number of azimuth steps	5
Signal bias	<0.5 dB
Operating temperature	−40 °C~40 °C

* Incidence angle off nadir; ** from nominal direction of 0°.

The SnowScat measurements were supported by detailed measurements of snow, soil, and atmospheric properties. Air, soil and snow temperature, as well as snow depth, were monitored by automated sensors, and weekly manual snow pit measurements provided an estimate of snow density, SWE, the snow stratigraphy (layering), and snow grain size in each layer. The maximum of SWE was up to 250 mm during 2009–2010 winter and 200 mm during 2010–2011 winter. Snow grain size was estimated by means of analyzing macro-photographs of snow grains taken against a reference grid. A representative sample of snow grains was manually removed from each layer for the purpose. Despite the acknowledged subjectivity and relatively high uncertainty of the measurement method, the grain size samples collected from the site have been shown to correlate with optical grain size measured using an integrating sphere instrument [46] as well as the microwave effective grain size derived from passive microwave observations by minimizing the simulated brightness temperature from model against the observed brightness temperature at 18 and 37 GHz in a cost function with the grain size as a free parameter in the model [47]. A Gamma Water Instrument (GWI), which measures the extinction of gamma rays emitted by an artificial gamma ray source over a given spectral band, was used to provide continuous information of Snow Water Equivalent. The instrument readings were calibrated against SWE provided by manual snow pit observations.

The average grain size measured from the *in situ* during 2009–2010 winter was smaller than that during 2010–2011 winter [44]. Using this information for the SWE estimation, the mean value of single scattering albedo in the cost function Equation (14) was set as 0.65 and 0.8 for the two seasons, respectively. In this study, these values were roughly determined by the simulated database shown in Table 1 where the corresponding simulated signals was most close to the first few measured backscattering of the snow season. The reference value of optical thickness at these two periods is taken to be 0.02 based on the simulated database. Considering the most common scope of albedo and optical thickness of snow, variance values of 0.15 and 0.02 are typical for these two variables, respectively. Based on *in situ* measurements, we assume the snow temperature as a constant value of -8 °C for the winter of 2009–2010 and -6 °C for the winter of 2010–2011.

5. Results and Analysis

5.1. A Comparison of Estimated and Measured SWE

The time series of retrieved SWE in 2010–2011 and 2009–2010 are shown in Figure 9 against SWE measured by the GWI instrument. Generally, the estimated SWE agrees well with GWI observations. During the winters of these two years, the rising trend of SWE can be accurately estimated through our retrieval algorithm. The RMSEs between the observed and the estimated SWE are 16.59 mm for winter in 2009–2010 and 19.70 mm for winter in 2010–2011, respectively. It should be noted that the backscattering measurement we used for winter in 2009–2010 is the mean backscattering data over the whole azimuth range. Although the mean backscattering data we used has a poorer performance than that in the azimuth range of 0° to 20° [44], the RMSE for the retrieved SWE is still less than 30 mm which is acceptable [48]. An obvious deviation between the inversion results and the measured values on 18 February 2011 is shown in Figure 9b and this is caused by the decreased soil background signal due to refreezing at snow surface [44].

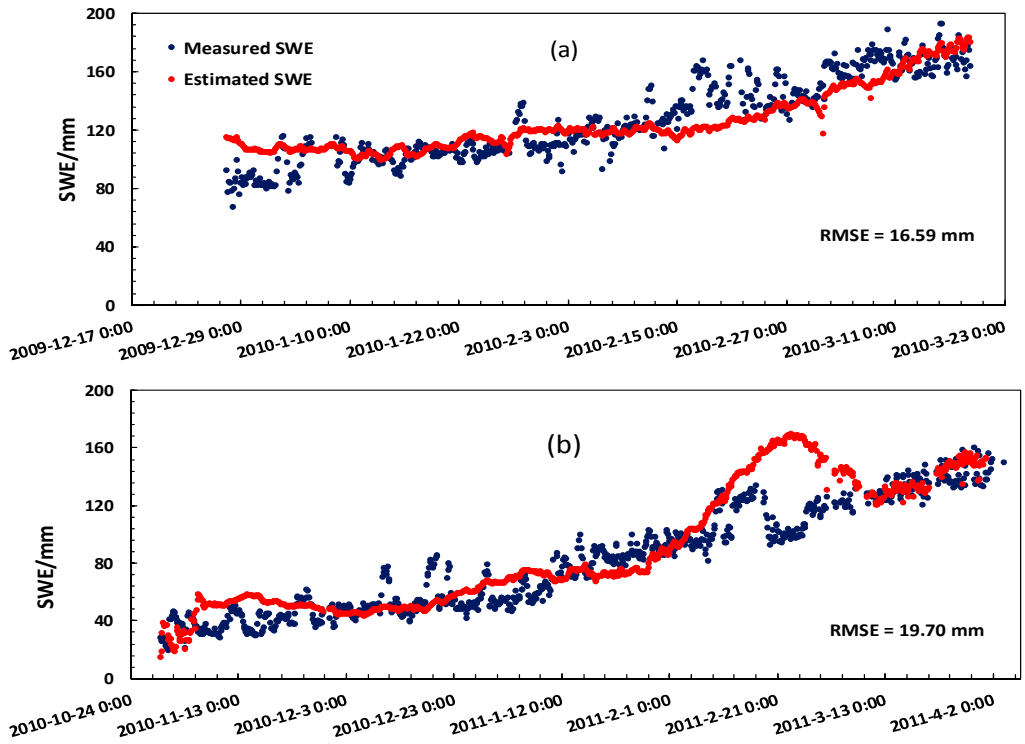

Figure 9. The time series of observed SWE (**black**) and estimated SWE (**red**) during: 27 December 2009–19 March 2010 (**a**); and 29 October 2010–4 April 2011 (**b**).

Soil melt/freeze events happened during end of October of 2010 resulting in some jitter in the retrievals (Figure 9b) at this time. The estimated SWE maintained a steady growth trend between 10 November and end of February when the air temperature stayed below 0 °C. However, there is an obvious discrepancy between the estimated SWE and the observed SWE from the end of February to the beginning of March in 2010–2011. This sudden variation can be explained by melt and re-freeze events of snow, causing an increase in backscattering in some azimuth directions [44].

5.2. Impact of Reference Value on SWE Estimation

In order to evaluate the impact of *a priori* values of albedo on the retrieval results, tests were performed with six different reference values and variances of effective albedo in the inversion. From Figure 10a, it can be seen that effective albedo with 0.2 variance shows a better result than that with 0.15 variance from 27 December 2009 to 29 January 2010. However, the measured SWE is underestimated from 30 January 2010 to 19 March 2010 when the variance of 0.2 is used. From Figure 10b, the retrieval with three albedo values and two variances of albedo is within observed SWE ± 30 mm from 29 October 2010 to 28 January 2011. The retrieval is overestimated with 0.2 variance later on. Generally, the retrieval with 0.65 effective albedo and 0.15 variance in 27 December 2009–19 March 2010 and 0.8 effective albedo and 0.15 variance in 29 October 2010–4 April 2011 shows overall agreement with the *in situ* observations of SWE.

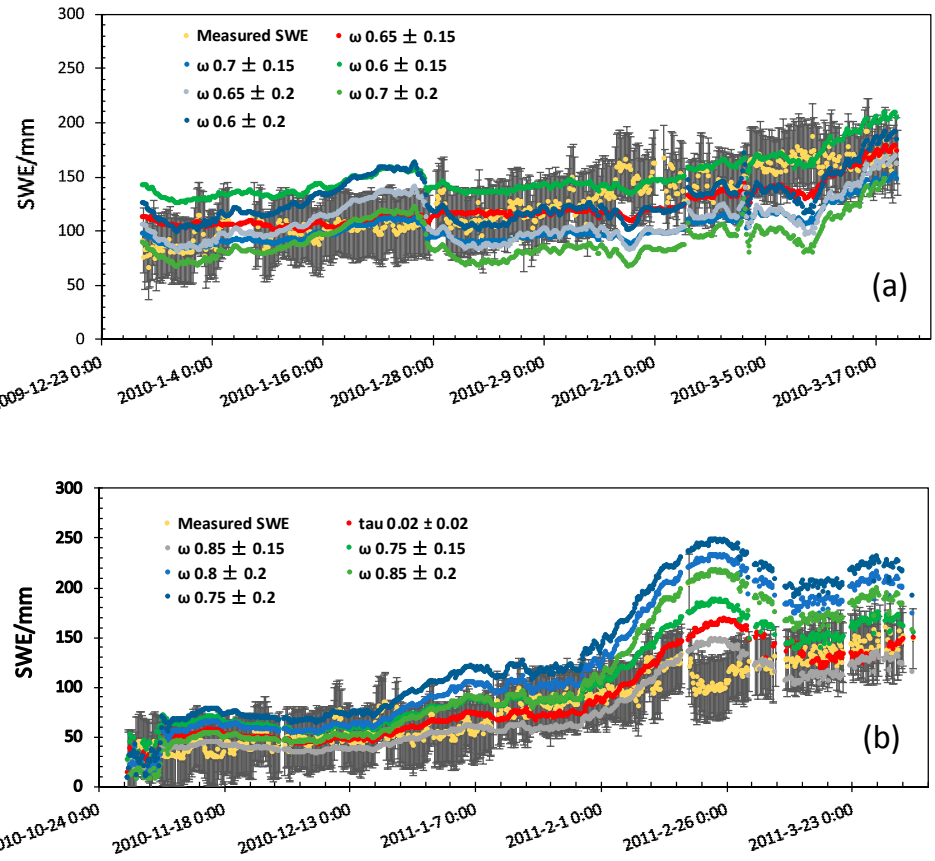

Figure 10. Retrieval using six different settings for the albedo reference values and variance values. Retrieved SWE (**red** dots) in comparison to measured SWE (**yellow** dots) with ±30 mm standard error (**black**) during: 27 December 2009–19 March 2010 (**a**); and 29 October 2010–4 April 2011 (**b**).

Table 6 shows RMSE between observed SWE and estimated SWE under different reference values and variances of effective albedo. In 2009–2010 winter, the difference of RMSE at different reference value is about 20 mm. However, in 2010–2011 winter, the difference reaches 45 mm. This can be

explained by the obvious discrepancy between the estimated SWE and the observed SWE from the end of February to the beginning of March in 2010–2011.

Assuming that the reference value of optical thickness is 0.02 in the cost function, we can get a fine inversion result during 27 December 2009–19 March 2010 and 29 October 2010–4 April 2011. What is more, the changes of reference variance value of optical thickness have very little effect on the estimation of SWE under this assumption.

Table 6. RMSE, Bias, R^2 at Different Reference Value and Variance of Albedo.

Time	Reference Value	Variance Value	RMSE/mm	Bias/mm	R^2
27 December 2009–19 March 2010	0.60	0.15	30.82	26.79	0.58
	0.65	0.15	19.70	16.06	0.79
	0.70	0.15	30.03	24.92	0.75
	0.60	0.20	28.14	21.62	0.78
	0.65	0.20	32.03	25.69	0.59
	0.70	0.20	43.05	35.86	0.58
29 October 2010–4 April 2011	0.75	0.15	30.58	23.74	0.81
	0.80	0.15	16.59	14.46	0.81
	0.85	0.15	21.06	15.10	0.81
	0.75	0.20	65.26	53.63	0.77
	0.80	0.20	52.33	40.48	0.77
	0.85	0.20	41.25	29.23	0.79

6. Summary and Conclusions

In this study, we developed a retrieval algorithm for SWE estimation from dual-frequency (X and Ku) backscattering measurements. This algorithm is based on a physical model in which the snow scattering is simulated by the bi-continuous-VRT model and the soil surface backscattering before snowfall is regarded as the ground backscattering under snow cover. To validate the accuracy of forward model, AIEM and Oh models were coupled to the bi-continuous-VRT under the measured soil surface parameters. By comparing the simulated results with the SARALPS-2007 experimental data, it was shown that in controlled conditions, this integrated model can generate reliably backscattering simulation for snow covered ground. We developed a new parameterization scheme for snow volume scattering in which the snow volume scattering is represented as a quadratic polynomial of the fist-order solution of snow volume radiative transfer equation. We also found good relationships for the single scattering albedo and snow optical thickness at X and Ku bands. The SWE is finally estimated through an iteratively minimized a cost function with prior constraints. Validation against two-year measurements of the SnowScat instrument from the NoSREx campaign shows that the estimated SWE with the presented algorithm has a root mean square error (RMSE) of 16.59 mm for winter in 2009–2010 and 19.70 mm for winter in 2010–2011, respectively.

As a physical model, the bi-continuous-VRT is more accurate in theory than the first or second order radiative transfer models and thus more promising considering application to the operational monitoring of snow scattering characteristics. However, prior knowledge of the size of snow particles is still needed in the present algorithm. The next step of the research is to evaluate the effect of particle size on the retrieval results, and to study the application of modeled grain size in the retrieval algorithm. In addition, the experimental area used in this study is relatively flat and clear of vegetation, while our algorithm does not take into account the influence of the terrain and vegetation at present. More effort needs to be devoted to applying this algorithm in mountainous and forested areas and this will be our future work.

Acknowledgments: This work was financially supported by the National Key Basic Research Program of China (Grant No. 2015CB953701), the National Natural Science Foundation of China (Grant No. 41401392) and the Strategic Priority Research Program for Space Sciences of the Chinese Academy of Sciences (Grant No. XDA04061200). SnowScat data were provided by the European Space Agency (ESA ESTEC Contract No. 22671/09/NL/JA/ef). We gratefully acknowledge part content of the Algorithm Theoretical Basis Document

(ATBD) for CoReH2O SWE algorithm provided by Helmut Rott at Institute for Meteorology and Geophysics, University of Innsbruck, Austria. Staff at the Finnish Meteorological Institute Arctic Research Centre are acknowledged for conducting *in situ* observations.

Author Contributions: Yurong Cui wrote the main manuscript text and prepared the figures and tables. Chuan Xiong contributed to the analysis and manuscript improvements. Lingmei Jiang, Bin Peng and Huixuan Li checked the manuscript. Juha Lemmetyinen was responsible for design of the field experiment and data processing. Jiancheng Shi proposed the initial design of the study. Tianjie Zhao, Dabin Ji and Tongxi Hu developed computer tools for remote sensing data.

Conflicts of Interest: The authors declare no conflict of interest.

References

1. Laghari, A.; Vanham, D.; Rauch, W. To what extent does climate change result in a shift in alpine hydrology? A case study in the Austrian Alps. *Hydrol. Sci. J.* **2012**, *57*, 103–117. [CrossRef]
2. Reinhardt, S.; Odland, A.; Pedersen, A. Calciphile alpine vegetation in Southern Norway: Importance of snow and possible effects of climate change. *Phytocoenologia* **2013**, *43*, 207–223. [CrossRef]
3. Berghuijs, W.; Woods, R.; Hrachowitz, M. A precipitation shift from snow towards rain leads to a decrease in streamflow. *Nat. Clim. Chang.* **2014**, *4*, 583–586. [CrossRef]
4. Barnett, T.P.; Adam, J.C.; Lettenmaier, D.P. Potential impacts of a warming climate on water availability in snow-dominated regions. *Nature* **2005**, *438*, 303–309. [CrossRef] [PubMed]
5. Li, L.; Simonovic, S. System dynamics model for predicting floods from snowmelt in North American prairie watersheds. *Hydrol. Process.* **2002**, *16*, 2645–2666. [CrossRef]
6. Jin, Z.; Charlock, T.P.; Yang, P.; Xie, Y.; Miller, W. Snow optical properties for different particle shapes with application to snow grain size retrieval and MODIS/CERES radiance comparison over Antarctica. *Remote Sens. Environ.* **2008**, *112*, 3563–3581. [CrossRef]
7. Vander Jagt, B.J.; Durand, M.T.; Margulis, S.A.; Kim, E.J.; Molotch, N.P. The effect of spatial variability on the sensitivity of passive microwave measurements to snow water equivalent. *Remote Sens. Environ.* **2013**, *136*, 163–179. [CrossRef]
8. Ulaby, F.T.; Stiles, W.H. The active and passive microwave response to snow parameters: 2. Water equivalent of dry snow. *J. Geophys. Res. Oceans (1978–2012)* **1980**, *85*, 1045–1049. [CrossRef]
9. Shi, J.; Dozier, J. Estimation of snow water equivalence using SIR-C/X-SAR. II. Inferring snow depth and particle size. *IEEE Trans. Geosci. Remote Sens.* **2000**, *38*, 2475–2488.
10. Ulaby, F.T.; Stiles, W.H.; Abdelrazik, M. Snowcover influence on backscattering from terrain. *IEEE Trans. Geosci. Remote Sens.* **1984**, 126–133. [CrossRef]
11. Shi, J.; Dozier, J. Estimation of snow water equivalence using SIR-C/X-SAR. I. Inferring snow density and subsurface properties. *IEEE Trans. Geosci. Remote Sens.* **2000**, *38*, 2465–2474.
12. Yueh, S.H.; Dinardo, S.J.; Akgiray, A.; West, R.; Cline, D.W.; Elder, K. Airborne Ku-band polarimetric radar remote sensing of terrestrial snow cover. *IEEE Trans. Geosci. Remote Sens.* **2009**, *47*, 3347–3364. [CrossRef]
13. Brogioni, M.; Macelloni, G.; Paloscia, S.; Pampaloni, P.; Pettinato, S.; Santi, E.; X'iong, C.; Crepaz, A. In Sensitivity analysis of microwave backscattering and emission to snow water equivalent: Synergy of dual sensor observations. In Proceedings of the XXXth URSI General Assembly and Scientific Symposium, Istanbul, Turkey, 13–20 August 2011; pp. 1–3.
14. Nghiem, S.V.; Tsai, W.-Y. Global snow cover monitoring with spaceborne Ku-band scatterometer. *IEEE Trans. Geosci. Remote Sens.* **2001**, *39*, 2118–2134. [CrossRef]
15. Shi, J.; Yueh, S.; Cline, D. On estimation of snow water equivalence using L-band and Ku-band radar. In Proceedings of the IEEE International Geoscience and Remote Sensing Symposium, IGARSS'03, Toulouse, France, 21–25 July 2003; pp. 845–847.
16. Shi, J. Snow water equivalence retrieval using X and Ku band dual-polarization radar. In Proceedings of the IEEE International Conference on Geoscience and Remote Sensing Symposium, Denver, CO, USA, 31 July–4 August 2006; pp. 2183–2185.
17. Pettinato, S.; Santi, E.; Brogioni, M.; Paloscia, S.; Palchetti, E.; Xiong, C. The potential of cosmo-skymed SAR images in monitoring snow cover characteristics. *IEEE Geosci. Remote Sens. Lett.* **2013**, *10*, 9–13. [CrossRef]

18. Rott, H.; Yueh, S.H.; Cline, D.W.; Duguay, C.; Essery, R.; Haas, C.; Heliere, F.; Kern, M.; Macelloni, G.; Malnes, E. Cold regions hydrology high-resolution observatory for snow and cold land processes. *Proc. IEEE* **2010**, *98*, 752–765. [CrossRef]
19. Shi, J.; Dong, X.; Zhao, T.; Liu, H.; Wang, Z.; Du, J.; Jiang, L.; Du, Y.; Ji, D.; Xiong, C. Observing earth's water cycle from space. In Proceedings of the SPIE International Asia-Pacific Environmental Remote Sensing Symposium, Beijing, China, 13–16 October 2014.
20. Shi, J.; Hensley, S.; Dozier, J. Mapping snow cover with repeat pass synthetic aperture radar. In Proceedings of the IEEE International Geoscience and Remote Sensing, IGARSS'97, Remote Sensing—A Scientific Vision for Sustainable Development, Singapore, 3–8 August 1997; pp. 628–630.
21. Guneriussen, T.; Høgda, K.A.; Johnsen, H.; Lauknes, I. InSAR for estimation of changes in snow water equivalent of dry snow. *IEEE Trans. Geosci. Remote Sens.* **2001**, *39*, 2101–2108. [CrossRef]
22. Tsang, L.; Pan, J.; Liang, D.; Li, Z.; Cline, D.W.; Tan, Y. Modeling active microwave remote sensing of snow using dense media radiative transfer (DMRT) theory with multiple-scattering effects. *IEEE Trans. Geosci. Remote Sens.* **2007**, *45*, 990–1004. [CrossRef]
23. Du, J.; Shi, J.; Rott, H. Comparison between a multi-scattering and multi-layer snow scattering model and its parameterized snow backscattering model. *Remote Sens. Environ.* **2010**, *114*, 1089–1098. [CrossRef]
24. Santi, E.; Brogioni, M.; Paloscia, S.; Pettinato, S.; Palchetti, E.; Xiong, C.; Crepaz, A. Combined use of experimental data and a multi-layer model for investigating the sensitivity of microwave indexes to snow parameters. In Proceedings of the IEEE International Geoscience and Remote Sensing Symposium-IGARSS, Melbourne, Australia, 21–26 July 2013.
25. Ding, K.-H.; Xu, X.; Tsang, L. Electromagnetic scattering by bicontinuous random microstructures with discrete permittivities. *IEEE Trans. Geosci. Remote Sens.* **2010**, *48*, 3139–3151. [CrossRef]
26. Chen, K.-S.; Wu, T.-D.; Tsang, L.; Li, Q.; Shi, J.; Fung, A.K. Emission of rough surfaces calculated by the integral equation method with comparison to three-dimensional moment method simulations. *IEEE Trans. Geosci. Remote Sens.* **2003**, *41*, 90–101. [CrossRef]
27. Morrison, K.; Rott, H.; Nagler, T.; Rebhan, H.; Wursteisen, P. The saralps-2007 measurement campaign on X and Ku-band backscatter of snow. In Proceedings of the IEEE International Geoscience and Remote Sensing Symposium IGARSS, Barcelona, Spain, 23–28 July 2007; pp. 1207–1210.
28. Oh, Y.; Sarabandi, K.; Ulaby, F.T. An empirical model and an inversion technique for radar scattering from bare soil surfaces. *IEEE Trans. Geosci. Remote Sens.* **1992**, *30*, 370–381. [CrossRef]
29. Fung, A.K.; Chen, K.-S. *Microwave Scattering and Emission Models for Users*; Artech House: Norwood, MA, USA, 2010.
30. Jiang, L.; Shi, J.; Tjuatja, S.; Dozier, J.; Chen, K.; Zhang, L. A parameterized multiple-scattering model for microwave emission from dry snow. *Remote Sens. Environ.* **2007**, *111*, 357–366. [CrossRef]
31. Rott, H.; Heidinger, M.; Nagler, T.; Cline, D.; Yueh, S. Retrieval of snow parameters from Ku-band and X-band radar backscatter measurements. In Proceedings of the IEEE International Geoscience and Remote Sensing Symposium IGARSS, Cape Town, South Africa, 12–17 July 2009.
32. Chang, W.; Tan, S.; Lemmetyinen, J.; Tsang, L.; Xu, X.; Yueh, S.H. Dense media radiative transfer applied to SnowScat and SnowSAR. *IEEE J. Sel. Top. Appl. Earth Obs. Remote Sens.* **2014**, *7*, 3811–3825. [CrossRef]
33. Fung, A.; Kuo, N. Backscattering from multi-scale and exponentially correlated surfaces. *J. Electromagn. Waves Appl.* **2006**, *20*, 3–11. [CrossRef]
34. Matzler, C. Microwave permittivity of dry snow. *IEEE Trans. Geosci. Remote Sens.* **1996**, *34*, 573–581. [CrossRef]
35. Xiong, C.; Shi, J. Simulating polarized light scattering in terrestrial snow based on bicontinuous random medium and monte carlo ray tracing. *J. Quant. Spectrosc. Radiat. Transf.* **2014**, *133*, 177–189. [CrossRef]
36. Xu, X.; Tsang, L.; Yueh, S. Electromagnetic models of co/cross polarization of bicontinuous/DMRT in radar remote sensing of terrestrial snow at X-and Ku-band for CoReH2O and SCLP applications. *IEEE J. Sel. Top. Appl. Earth Obs. Remote Sens.* **2012**, *5*, 1024–1032. [CrossRef]
37. Xiong, C.; Shi, J.; Lemmetyinen, J. Refinement of the X and Ku band dual-polarization scatterometer snow water equivalent retrieval algorithm. In Proceedings of the IEEE International Geoscience and Remote Sensing Symposium (IGARSS), Quebec City, QC, Canada, 13–18 July 2014; pp. 2419–2422.
38. Ulaby, F.T.; Moore, R.K.; Fung, A.K. *Microwave Remote Sensing*; Artech House: Reading, MA, USA, 1982; Volume 2.

39. Gabarró, C.; Portabella, M.; Talone, M.; Font, J. Toward an optimal SMOS ocean salinity inversion algorithm. *IEEE Geosci. Remote Sens. Lett.* **2009**, *6*, 509–513. [CrossRef]
40. Qi, Z.; Wei, E. Analysis of cost functions for retrieving sea surface salinity. *J. Ocean Univ. China* **2012**, *11*, 147–152. [CrossRef]
41. Rott, H.; Nagler, T.; Voglmeier, K.; Kern, M.; Macelloni, G.; Gai, M.; Cortesi, U.; Scheiber, R.; Hajnsek, I.; Pulliainen, J. Algorithm for retrieval of snow mass from Ku-and X-band radar backscatter measurements. In Proceedings of the IEEE International Geoscience and Remote Sensing Symposium (IGARSS), Munich, Germany, 22–27 July 2012; pp. 135–138.
42. Tsang, L.; Kong, J.A.; Shin, R.T. *Theory of Microwave Remote Sensing*; Wiley: New York, NY, USA, 1985.
43. Matzler, C. Microwave properties of ice and snow. In *Solar System Ices*; Springer: Dordrecht, The Netherlands, 1998; pp. 241–257.
44. Lemmetyinen, J.; Kontu, A.; Pulliainen, J.; Vehviläinen, J.; Rautiainen, K.; Wiesmann, A.; Mätzler, C.; Werner, C.; Rott, H.; Nagler, T.; *et al.* Nordic snow radar experiment. *Geosci. Instrum. Method Data Syst. Discuss.* **2016**, *2016*, 1–23. [CrossRef]
45. Werner, C.; Wiesmann, A.; Strozzi, T.; Schneebeli, M.; Mätzler, C. The snowscat ground-based polarimetric scatterometer: Calibration and initial measurements from davos switzerland. In Proceedings of the IEEE International Geoscience and Remote Sensing Symposium (IGARSS), Honolulu, HI, USA, 25–30 July 2010; pp. 2363–2366.
46. Leppänen, L.; Kontu, A.; Vehviläinen, J.; Lemmetyinen, J.; Pulliainen, J. Comparison of traditional and optical grain-size field measurements with snowpack simulations in a taiga snowpack. *J. Glaciol.* **2015**, *61*, 151–162. [CrossRef]
47. Lemmetyinen, J.; Derksen, C.; Toose, P.; Proksch, M.; Pulliainen, J.; Kontu, A.; Rautiainen, K.; Seppänen, J.; Hallikainen, M. Simulating seasonally and spatially varying snow cover brightness temperature using hut snow emission model and retrieval of a microwave effective grain size. *Remote Sens. Environ.* **2015**, *156*, 71–95. [CrossRef]
48. Kern, M. *CoReH2O-Cold Regions Hydrology High-Resolution Observatory. Candidate Earth Explorer Core Mission. Report for Assessment*; ESA SP: Noordwijk, The Netherlands, 2008; Volume 1313.